International Journal of Plasticity 48 (2013) 111–124

Contents lists available at SciVerse ScienceDirect

International Journal of Plasticity

journal homepage: www.elsevier.com/locate/ijplas

Homogenized constitutive and fatigue nucleation models from crystal plasticity FE simulations of Ti alloys, Part 2: Macroscopic probabilistic crack nucleation model

Masoud Anahid [a], Somnath Ghosh [b,*]

[a] Department of Mechanical Engineering, The Ohio State University, United States
[b] Department of Civil Engineering, Johns Hopkins University, United States

ARTICLE INFO

Article history:
Received 4 September 2012
Received in final revised form 31 January 2013
Available online 27 February 2013

Keywords:
Probabilistic crack nucleation model
Titanium alloys
Homogenization
Dislocation pile-up

ABSTRACT

This is the second of a two-part paper aimed at the developing macroscopic models of fatigue deformation and failure in polycrystalline Ti alloys. In this part, a probabilistic crack nucleation model is developed for predicting damage nucleation in macroscopic computations of the structural components from rigorous microscopic analyzes. Inputs to this model include morphological characteristics of the microstructure at any material point along with the local stress/strain state. This stress-state, needed to trigger this model, can be obtained from finite element analysis using the homogenized, anisotropic plasticity constitutive (HAPC) model developed in part 1 (Ghosh et al., in press). A deterministic functional form, relating time for macroscopic crack nucleation to the macroscopic stress state and microstructural characteristic parameters, is derived from rigorous crystal plasticity FE simulations of representative volume element of a bi-crystal system that implements a physics-based grain level crack nucleation model. Subsequently, a probabilistic model for expected crack nucleation in the macroscopic (structural) scale is generated from this functional form. The probabilistic model has a direct connection to the mechanisms of microstructural crack nucleation and can be obtained from macroscopic FE analysis with knowledge of statistics of the local microstructure.

1. Introduction

Fatigue crack nucleation and life in titanium alloys such as Ti-6242 vary considerably from one specimen to another, due to their nonuniform underlying microstructure that affects localized deformation and damage characteristics (Bache, 2003; Bache et al., 1997; Sinha et al., 2004). Conventional fatigue analysis methods e.g., the stress-life, strain-life approaches, or damage tolerant approaches (Suresh, 1998; Laird, 1976; Fleck et al., 1994; Coffin, 1973; Paris, 1964), where phenomenological models obtained from extensive testing of specimens are used to predict life, do not adequately account for the effect of microstructure or evolving mechanisms.

Recent years have seen a paradigm shift towards the use of material microstructure-based detailed mechanistic models for predicting fatigue crack nucleation and propagation. These mechanistic approaches implement crystal plasticity finite element or (CPFE) simulations of polycrystalline microstructures (Sinha and Ghosh, 2006; Goh et al., 2001; Sackett et al., 2007; Bridiera et al., 2009; Mineur et al., 2000; McDowell and Dunne, 2010; Ghosh et al., 2011) to develop fatigue life models. They are considered promising alternatives to the conventional models. The fatigue crack nucleation model for Ti-6242

* Corresponding author. Address: 3400 N. Charles St., Baltimore, MD 21218, USA. Tel.: +1 410 516 7833; fax: +1 410 516 7473.
E-mail address: sghosh20@jhu.edu (S. Ghosh).

0749-6419/$ - see front matter © 2013 Elsevier Ltd. All rights reserved.
http://dx.doi.org/10.1016/j.ijplas.2013.02.008

alloy under cyclic loading in (Kirane and Ghosh (2008); Kirane et al. (2009); Anahid et al. (2009)) uses the results of CPFE simulations to predict the nucleation sites and time in polycrystalline aggregates. This model assumes that dislocation pileup in neighboring soft grains follows the same distribution function as for single slip, which restricts its application. To overcome this limitation, an experimentally validated, microstructure-based non-local crack nucleation model has been developed in (Anahid et al., 2011; Ghosh et al., 2011) for polycrystalline alloys subject to fatigue loading. This nonlocal model accounts for the cumulative effect of slip on multiple slip systems, and involves evolving mixed mode stresses in the grain along with dislocation pileups in contiguous grains. It requires the grain-level distributions of stresses and plastic strains from CPFE simulations with evolving deformation. Fatigue life predictions using the results of CPFE simulations have also been performed in (Bennett and McDowell, 2003; Sinha and Ghosh, 2006; Turkmen et al., 2003; Bieler et al., 2009). Although CPFE simulations accurately depict the deformation behavior, these grain-level models typically capture the behavior of only a small region of the microstructure containing at most thousands of grains. Hence, it is impossible to make reliable predictions of fatigue failure from FEM simulations at the structural scale using these models. Various probabilistic methods have been developed to provide uncertainty quantification for life prediction. The DARWIN (Design Assessment of Reliability with Inspections) code (McClung et al., 2004) has been developed to calculate the risk of fracture caused by the specific damage sources and the total accumulated risk over the projected lifetime. A microstructure-sensitive extreme value probabilistic framework has been developed in (Przybyla and McDowell, 2010; Przybyla and McDowell, 2011) to study the fatigue crack formation in different superalloys. Probabilistic life prediction models have also been presented in (Liu and Mahadevan, 2009; Owolabi et al., 2010).

This second of the two part paper, develops a macroscopic probability-based fatigue nucleation model at the structural scale, from detailed microscopic fatigue crack nucleation simulations in polycrystalline microstructures of Ti alloys. The model utilizes the homogenization-based macroscopic anisotropic constitutive model, developed in part 1 of this paper (Ghosh et al., in press). This constitutive model incorporates functional forms of microstructural parameters like orientation or Schmid factor, misorientation, and grain sizes to predict the distribution of stress and plastic strain distribution in the structure. This stress/strain distribution is necessary for predicting macroscopic crack nucleation at the structural level with connection to the underlying microstructure. For developing the crack nucleation model, a wide range of CPFE simulations are first conducted on two grain representative volume elements, with varying morphology and crystallography. The grain level crack nucleation model in (Anahid et al., 2011; Ghosh et al., 2011) is used to arrive at a functional form relating the time to crack initiation (t_f) with the macroscopic stress level and microstructural parameters. Next the functional form is used to develop a probabilistic model for expected crack nucleation at any location in the structural scale. The local morphology, e.g. distribution functions of orientation, misorientation and grain size should be known at these locations.

In the organization of this paper, the experimentally validated grain-level crack nucleation model of (Anahid et al., 2011) is summarized in Section 2. In Section 3, the grain-level crack nucleation of single phase Ti alloys is related to the microstructural properties and applied stress. A probabilistic crack nucleation model is presented in Section 4 for Ti alloys at the structural scale.

2. Grain level non-local crack nucleation model

Various experimental studies have been made for this problem with different inferences. In a recent study on the facet formation in near-α titanium in (Pilchak and Williams, 2011), it was observed that dwell fatigue cracking occurred at the intersection of an inclined basal slip band with a $10\bar{1}7$ plane that was nearly perpendicular to the loading direction. The basal slip band was in a plane with high Schmid factor which corresponded to a soft grain. On the other hand, the grain with $10\bar{1}7$ plane nearly perpendicular to the loading direction is a hard grain. This finding emphasizes the fact that the crack nucleation under dwell fatigue is a result of an interaction between the hard/soft grain combination. For static loading in air, the crack was found to nucleate on a facet inclined $\sim 23^{\circ}$ to the loading direction, nearly parallel to the basal plane. Extensive experimental studies on the relation between crack initiation and crystallographic orientations in samples of Ti-6242 have also been conducted in (Sinha et al., 2006a; Sinha et al., 2006b) using quantitative tilt fractography and Electron Back Scattered Diffraction (EBSD) techniques in SEM. Failure sites are found to be predominantly at those locations where the basal plane is nearly orthogonal to the principal loading direction (Sinha et al., 2006a). In (Sinha et al., 2006b), the angle θ_c between the loading axis and the crystallographic c-axis at the failure site has been found to be quite small ($\sim 0^{o} - 30^{o}$). Furthermore, the failure site shows a low prism activity with the Schmid factor $\sim 0 - 0.1$ and a moderate basal activity with Schmid factor $\sim 0.3 - 0.45$. However, the region surrounding the failure site has a high prismatic and basal activity with Schmid factor ~ 0.5. The overall inference from these observations is that while crack nucleation occurs in a region that is unfavorably oriented for slip (hard grain), it is surrounded by grains that are favorably oriented for slip (soft grain). These observations also suggest, time-dependent accumulation of stress in the hard oriented grains due to load shedding with increasing plastic deformation in the surrounding soft grains. This is responsible for crack nucleation in Ti alloys under creep and dwell loading. In this paper, the proposed grain-level transgranular crack nucleation model is based on microscopic experimental observations on polycrystalline Ti alloys, made in (Sinha et al., 2006a; Sinha et al., 2006b). The authors acknowledge, that the model may change depending on the accepted form of experimentally observed crack nucleation modes.

The development of the grain-level crack nucleation model has been described in details in (Anahid et al., 2011; Ghosh et al., 2011). Since, this is used in this work it is summarized in this paper. The intra-granular crack nucleation model

assumes that a wedge crack nucleates in a neighboring grain as dislocations approach the grain boundary. An edge dislocation, which is an extra half plane of atoms wedged between two complete planes, is equivalent to a micro-crack with opening displacement of one atomic spacing b. As more dislocations are piled up at the grain boundary, the crack opening increases in size, as shown in Fig. 1(a). The crack opening displacement corresponds to the closure failure along a circuit surrounding the piled-up dislocations. If n edge dislocations of Burger's vector b, contribute to the formation of a micro-crack, a wedge with opening displacement $B = nb$ is produced. It should be noted that while the dislocations are piled up at the grain boundary of a soft grain, the wedge crack initiates in the adjacent hard grain as shown in Fig. 1(b).

The micro-crack length c in Fig. 1(a) can be considered as the length-scale beyond which, the disturbance in the lattice structure of the hard grain subsides. This disturbance is caused by extra half-planes of atoms in the soft grain. The equilibrium length c of a wedge crack with an opening displacement B has been related to the elastic properties and surface energy γ_s in (Stroh, 1954) as:

$$c = \frac{G}{8\pi(1-\nu)\gamma_s}B^2 \tag{1}$$

where ν is the Poisson's ratio and G is the shear modulus.

The wedge crack is initially stable. As more dislocations enter the crack, the crack opening size increases, causing the crack length to grow. Additionally, the stress in the hard grain across the micro-crack also aids in opening up the crack. The multi-axial stress acting on the micro-crack surface is a combination of normal and shear stresses as shown in Fig. 1(b). It is assumed that cracks nucleate from the tip, when the mixed mode stress intensity factor K_{mix} exceeds a critical value, K_c. K_{mix} is expressed in terms of normal stress intensity factor K_n and shear stress intensity factor K_t as:

$$K_{mix}^2 = K_n^2 + \beta K_t^2 \tag{2}$$

where β is a shear stress factor, which is used to assign different weights to the normal and shear traction components for mixed mode. In (Ruiz et al., 2001), β is defined as the ratio of the shear to normal fracture toughness of the material, i.e. $\beta \approx K_{nc}/K_{tc}$. A value of $\beta = 0.7071$ has been suggested for Ti-64 alloys in (Parvatareddy and Dillard, 1999). Using the definitions for stress intensity factors $K_n = < T_n > \sqrt{\pi c}$ and $K_t = T_t\sqrt{\pi c}$ and noting that the micro-crack grows when $K_{mix} \geqslant K_c$, the hard grain crack nucleation criterion, ahead of dislocation pile-ups in adjacent soft grain is stated as:

$$T_{eff} = \sqrt{< T_n >^2 + \beta T_t^2} \geqslant \frac{K_c}{\sqrt{\pi c}} \tag{3}$$

or equivalently

$$R = T_{eff}.\sqrt{c} \geqslant R_c, \quad \text{where } R_c = \frac{K_c}{\sqrt{\pi}} \tag{4}$$

T_{eff} is an effective stress for mixed mode crack nucleation. It is expressed in terms of the stress component normal to the crack surface $T_n = \sigma_{ij} n_i^b n_j^b$ and the tangential stress component $T_t = \|\mathbf{T} - T_n \mathbf{n}^b\|$. Here $\mathbf{T}$ is the stress vector on the crack surface, σ_{ij} is the Cauchy stress tensor and n_i^b are the components of unit outward normal to the crack surface. Only the tensile normal stress $< T_n >$, represented by the McCauley bracket $<>$, contributes to the effective stress responsible for crack opening.

Sensitivity analysis with different values of β indicate that T_{eff} is not very sensitive to β for hard grains with $< c >$ axis almost parallel to the loading direction, since $T_n \gg T_t$. It is worth noting that the stress components in Eq. (3) are remote applied stresses. However, since the typical values of c that cause unstable cracking are of the order of nanometers, while

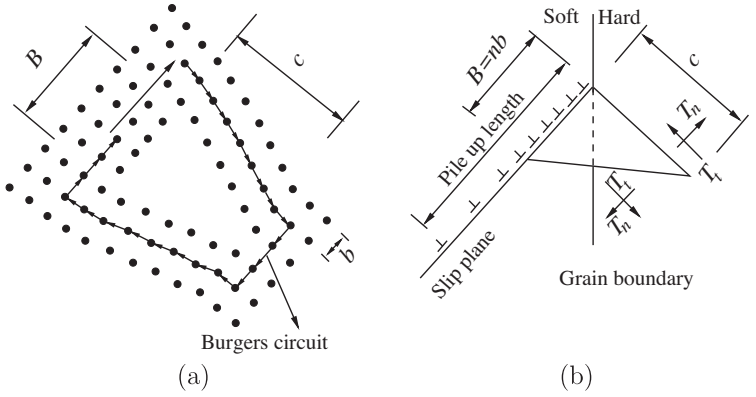

Fig. 1. (a) A wedge crack with opening displacement of $4b$, produced by coalescence of four dislocations, (b) nucleation of a wedge crack in the hard grain resulting from a dislocation pile-up in the soft grain.

the typical grain size is of the order of microns, it is reasonable to consider the maximum stress at the hard grain boundary as the remote stress. As more dislocations are added to the pile-up with time, the wedge crack opening displacement and length increase. This implies that a smaller T_{eff} is needed to initiate a crack with increasing plastic deformation and pile-up. This contributes to the non-locality aspect of the crack nucleation criterion.

The parameter R_c in Eq. (4) depends on the elastic properties as well as on the critical strain energy release rate G_c. It has the units of stress intensity factor ($\mathrm{MPa}\sqrt{\mu\mathrm{m}}$). In (Anahid et al., 2011) R_c has been calibrated by using data extracted from a combination of ultrasonic experiments using acoustic microscopy and CPFE simulations on an image-based microstructure. The calibrated value for Ti-6242 specimen is found to be $R_c = 178.7\mathrm{MPa}\sqrt{\mu\mathrm{m}}$.

2.1. Numerical implementation of the crack nucleation criterion

Crack nucleation is examined on different planes in the hard grain of the polycrystalline microstructure. Determination of the micro-crack length c for Eq. (4), requires the evaluation of the opening displacement B in Eq. (1) that in turn necessitates the determination of distribution of dislocations inside the soft grain. The crystal plasticity model discussed in the first part of this paper (Ghosh et al., in press) does not explicitly have dislocation density as a state variable. To overcome this limitation, plastic strains and their gradients that are available from the results of the CPFE simulations are used to estimate the micro-crack opening displacement B. The wedge opening displacement in Fig. 1(a) is equal to the closure failure along a circuit surrounding the piled-up edge dislocations on one slip plane. This can be extended to a generalized 3D representation of dislocations for multiple slip systems. The corresponding closure failure, which is manifested as the crack opening displacement, is a vector quantity. In the dislocation glide model, the lattice incompatibility can be measured by the closure failure of a line integral along a Burgers circuit $\bar{\Gamma}$ in the intermediate configuration. Closure failure is equivalent to the net Burgers vector $\mathbf{B}$ of all dislocations passing through the region $\bar{\Omega}$, bounded by the circuit. The Burgers vector can be mapped to a line integral along a referential circuit, Γ using the plastic deformation gradient $\mathbf{F}^p$. Using Stoke's theorem, the closure failure is related to the surface integral of the curl of $\mathbf{F}^p$ over a referential surface Ω as:

$$\mathbf{B} = \oint_{\bar{\Gamma}} d\bar{\mathbf{x}} = \oint_{\Gamma} \mathbf{F}^p d\mathbf{X} = \int_{\Omega} \Lambda . \mathbf{n} d\Omega \tag{5}$$

where $\mathbf{n}$ is the unit normal to the surface Ω and Λ is the Nye's dislocation tensor defined in the first part. Components of Λ are evaluated at each quadrature point using shape function based interpolation of nodal values of $\mathbf{F}^p$, as described in (Anahid et al., 2009).

The closure failure obtained from Eq. (5) can make any arbitrary angle with respect to the surface, depending on the type of dislocations passing through $\bar{\Omega}$. It also depends on the angle between dislocation line and the surface. For a pure edge dislocation with the dislocation line perpendicular to $\bar{\Omega}$, the closure failure, $\mathbf{B}$ lies in the plane. If the dislocation line is not perpendicular to $\bar{\Omega}$, the closure failure does not lie in the plane. For a pure screw dislocation with a dislocation line perpendicular to $\bar{\Omega}$, $\mathbf{B}$ is also perpendicular to the plane. For a mixed type of dislocation with edge and screw components, $\mathbf{B}$ is neither perpendicular nor parallel to Ω.

Assume that there is a point on the hard-soft grain boundary (point A in Fig. 2(a)), which impedes all dislocations generated from different sources in the soft grain. There are different planes with different normal vectors, which contain point A. The closure failure caused by dislocations piercing each of these planes depends on the normal, $\mathbf{n}$ based on Eq. (5). The stresses on each of the resulting micro-cracks are also different. Consequently, there are different possible competing micro-cracks with dissimilar stress intensity factors at point A. The crack with the highest mixed-mode stress

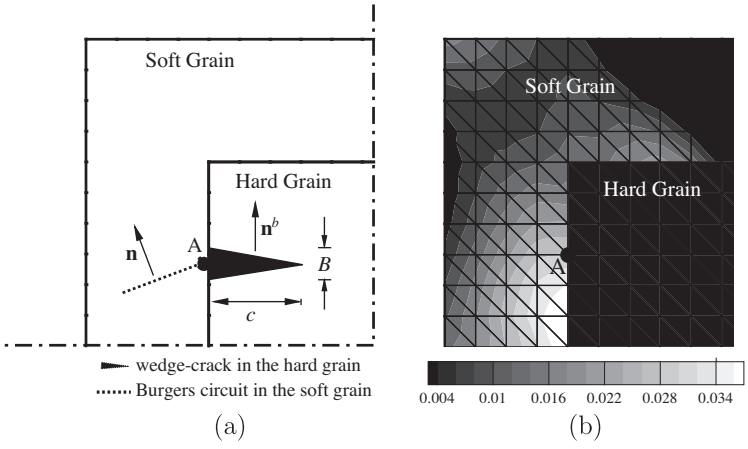

Fig. 2. (a) Wedge-crack in the hard grain as a result of dislocation pileup in adjacent soft grain, (b) distribution of the norm of Nye's dislocation tensor inside a representative hard-soft grain combination.

intensity factor is considered as the critical one. If the unit normal to the area surrounded by a Burgers circuit containing point A in Fig. 2(a) is denoted by $\mathbf{n}$, the size of crack opening displacement B is calculated using Eq. (5) as:

$$B = \|\Lambda.\mathbf{n}\| \tag{6}$$

This is used in Eq. (1) to estimate the crack length c. Neglecting the effect of screw dislocations on the wedge crack opening, the unit normal to the wedge crack surface is obtained as:

$$\mathbf{n}^b = \frac{\Lambda.\mathbf{n}}{B} \tag{7}$$

It should be noted that the wedge crack surface does not necessarily correspond to a slip plane in the hard grain, since $\mathbf{n}$ in Eq. (7) can correspond to any arbitrary direction.

The mixed mode stress intensity factor that corresponds to the wedge crack produced by dislocations passing through the unit area surface with unit normal of $\mathbf{n}$ is obtained as:

$$K_{mix} = T_{eff}\sqrt{\pi c} \tag{8}$$

This procedure is executed for all possible $\mathbf{n}$ vectors in 3D space. The vector $\mathbf{n}_{cr}$, which yields the highest stress intensity factor, is considered as the critical normal vector. The critical crack opening displacement at the hard-soft grain boundary is then obtained as $\mathbf{B}_{cr} = \Lambda \cdot \mathbf{n}_{cr}$. This relation is true when all dislocations are concentrated in a very small portion of the soft grain, surrounding the point A. However, dislocations are distributed in the entire soft grain. Fig. 2(b) shows the contour of the norm of Nye's dislocation tensor in a representative hard-soft grain combination. Values of Λ are available at the integration points of all the tetrahedron elements within the soft grain from the CPFE simulations. Each element I contains its own dislocations quantified by Nye's dislocation tensor Λ_I in that element. Dislocations associated with element I produce a crack opening displacement that may be estimated as:

$$\mathbf{B}_I = W_I A_I \Lambda_I.\mathbf{n}_{cr} \tag{9}$$

Here A_I is the surface area associated with tetrahedron element I, into which the dislocations penetrate. The area is estimated by assuming an equivalent spherical domain with the same volume as the element. The center of this sphere is assumed to coincide with the element integration point. Assuming that the plane containing the Burgers circuit in the element I passes through the integration point, A_I is equal to the circular cross-sectional area passing through the center of sphere, and is expressed as:

$$A_I = \pi R_I^2 = 1.77(V_I)^{\frac{2}{3}} \quad \text{where } R_I = \sqrt[3]{\frac{3}{4\pi}V_I}, \tag{10}$$

V_I is the element volume and R_I is sphere's radius. A weighting parameter W_I is introduced to $\mathbf{B}_I$ to account for the diminishing effect of dislocations on the crack opening displacement with distance. The weighting parameter for the I-th element integration point is chosen according to a formula proposed in (Engelen et al., 2003) as:

$$W_I = exp(-r_I^2/2l^2), \text{ st. } W_I \to 0 \text{ for } r \geqslant l_{cr}; \quad W_I = 1 \text{ for } r_I = 0 \tag{11}$$

where r_I is the distance from point A in Fig. 2(b) and l_{cr} is a critical radius. Thus the magnitude of the crack opening displacement B, accounting for the contribution of all elements in the soft grain on the hard grain crack, may be stated as:

$$B = \|\mathbf{B}\| = \|\sum_I \mathbf{B}_I\| = \|\sum_I W_I A_I \Lambda_I.\mathbf{n}_{cr}\| \tag{12}$$

Defining an effective dislocation tensor as:

$$\mathbf{D}_{eff} = \sum_I W_I A_I \Lambda_I \tag{13}$$

Eq. (12) can be rewritten as:

$$B = \|\mathbf{D}_{eff}.\mathbf{n}_{cr}\| \tag{14}$$

The micro-crack length c is then derived from the crack opening displacement in Eq. (1) as:

$$c = \frac{G}{8\pi(1-\nu)\gamma_s}\|\mathbf{D}_{eff}.\mathbf{n}_{cr}\|^2 \tag{15}$$

Inserting material properties for Ti alloys as $G = 48GPa$, $\nu = \frac{1}{3}$ and $\gamma_s = 5$ N/m, this relation is rewritten as:

$$c = 573 \times 10^6 \|\mathbf{D}_{eff} \cdot \mathbf{n}_{cr}\|^2 \text{ (in m)} \tag{16}$$

The unit normal to the wedge crack surface in the hard grain is

$$\mathbf{n}^b = \frac{\mathbf{D}_{eff}.\mathbf{n}_{cr}}{\|\mathbf{D}_{eff}.\mathbf{n}_{cr}\|} \tag{17}$$

The effective traction T_{eff} is updated using the procedure described in Section 2 and $\mathbf{n}^b$ from Eq. (17). Finally, T_{eff} and c are used in Eq. (4) to calculate the effective nucleation variable R. R is checked for every grain pair in the CPFE model in the post-processing stage as follows:

- For each grain pair in the microstructure, the hard and soft grain is decided based on the amount of plasticity and stress concentration in each constituent grain.
- For each grain in the pair, tetrahedral elements with a triangular edge on the shared boundary are determined. The nodes of these triangles are the common nodes between the two grains.
- For each common node on the shared boundary, the critical normal vector $\mathbf{n}_{cr}$, and the stress intensity factor associated with this normal vector are obtained using a procedure mentioned earlier in this section. The Nye's dislocation tensor at each common node, which is required to estimate c, is obtained from the integration points in the surrounding elements inside the soft grain. A weighted averaging scheme is used for this purpose as described in (Anahid et al., 2009). Correspondingly, the nodal values of stress components are calculated from integration points in the surrounding elements inside the hard grain.
- The common node with the highest stress intensity factor, which corresponds to the aforementioned point A in this section, is chosen. This point does not necessarily have the highest norm of Nye's dislocation tensor among the common nodes. Consequently, the variable R is obtained for the grain-pair using Eqs. (10)–(17).

This grain-based crack nucleation model has been satisfactorily calibrated and validated for Ti alloys in (Anahid et al., 2011) using data available from acoustic microscopy experiments for monitoring crack evolution in fatigue experiments. This model at the microstructural level will now be used to develop a macroscopic probabilistic model of crack nucleation.

3. Sensitivity analysis of crack nucleation in two-grain CPFEE analysis

Load shedding phenomenon, due to strength mismatch between hard and soft grains, is primarily responsible for crack initiation in titanium alloys. The soft grains have $< c >$-axis at nearly 45^o orientation with respect to the deformation axis, while the hard grains have $< c >$-axis nearly parallel to the deformation direction. A two-grain hard-soft pair of single phase α-Ti alloys is studied to relate the crack nucleation phenomenon to microstructure properties and the applied stress. Specifically, the time to crack initiation t_f for the grain pair is assumed to depend on the following factors.

- Schmid factor of the soft grain SF
- Misorientation between hard and soft grains θ_{mis}
- Soft grain size D
- Macroscopic stress level P

The Schmid factor for a slip system and the misorientation between two adjacent grains have been defined in the first part of this paper. The finite element CPFE model of the two-grain RVE consists of a solid inner cube representing a primary α hard grain contained in an exterior annular cube representing the softer primary α grain as shown in Fig. 3 (a). The two regions in the CPFE model can differ in their orientation and size. For creep analysis, a load of magnitude P is applied to the system along the y axis. The loading axis is assumed to coincide with the $< c >$-axis of the hard grain, for which all basal and prismatic Schmid factors are zero. The orientation of the soft grain is chosen in such a way that a specified Schmid factor for the soft grain and a specified misorientation between hard and soft grains is achieved. The ratio of soft to hard grain size is 2.5. The inner cube (hard grain) is discretized into a mesh of 1296 four-noded linear tetrahedron elements, while the outer cube (soft grain) has a mesh of 15168 elements. Prior to accepting this mesh (with total number of 16464 elements) for CPFE simulations leading to crack nucleation, a convergence study is conducted to examine mesh sensitivity. In addition to the aforementioned mesh system, a more refined mesh with 34992 linear tetrahedron elements is used for the convergence study. A creep simulation study is conducted for both these models for 1000 s with an applied load of 650 MPa in the Y-direction. The local stress component in the loading direction is compared for various sections of the FE models at the end of 1000 s. A plot comparing the distribution of the stress along a section parallel to the Z-axis is shown in Fig. 3(b). It shows good agreement in the local stresses for the two mesh densities. Thus, the 16464-element mesh is taken to be a converged model for the loading considered and is used for the microscopic fatigue crack nucleation simulations.

Several CPFE simulations with different stress levels are conducted on the two grain CPFE model with different combinations of microstructural parameters. For each RVE, results of CPFE simulations are post-processed to calculate the time to nucleate the first crack t_f. This corresponds to the state for which the maximum value of the nucleation parameter in Eq. (4) at a point in the grain reaches the condition $R_{max} = R_c$. In (Anahid et al., 2011) the critical value of the parameter has been determined to be $R_c = 178.7\ \text{MPa}\sqrt{\mu\text{m}}$ for the titanium alloy under consideration. Fig. 4 depicts a typical plot for the maximum R in the model as a function of time, in the uniaxial creep study. This parametric study is used to establish a functional form of t_f in terms of the stress level and the microstructural parameters as:

$$t_f = t_f(SF, \theta_{mis}, D, P) \tag{18}$$

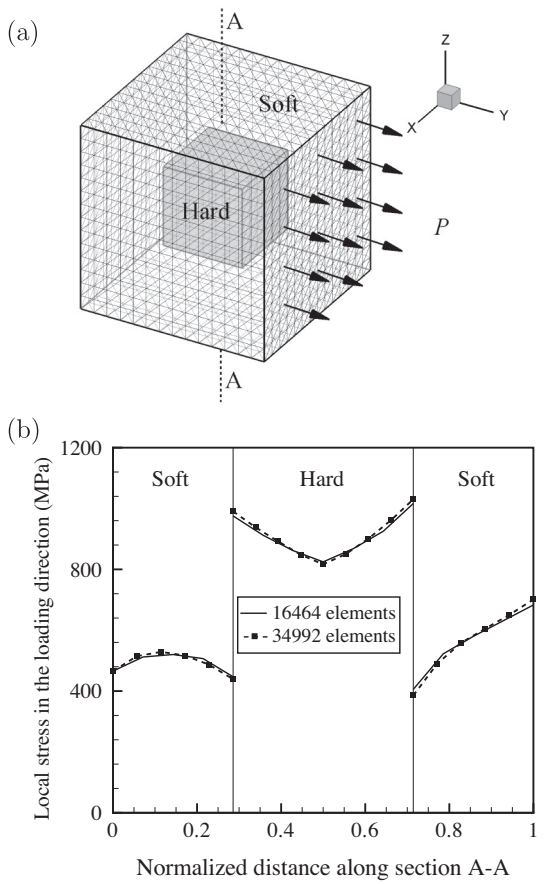

Fig. 3. (a) Crystal plasticity FE model of the microstructural two grain system used for crack nucleation sensitivity studies, (b) distribution of the loading direction stress (σ_{22}) along a section parallel to the z-axis at the end of 1000 s, for a creep simulation of two microstructural RVE models with different mesh densities.

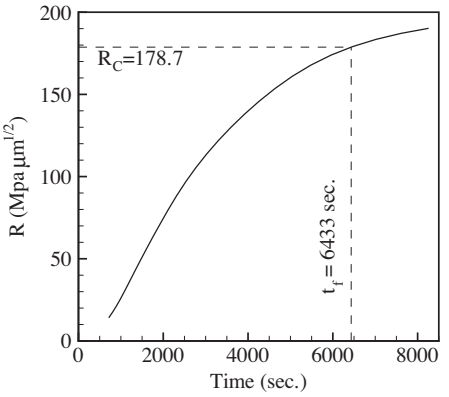

Fig. 4. The evolution of the nucleation parameter R with time. This corresponds to a two-grain RVE with the soft grain size $D = 7.5$ m, Schmid factor $SF = 0.5$, misorientation $\theta_{mis} = 45^o$ and load $P = 650$ MPa.

The function t_f represents the effect of Schmid factor, misorientation, grain size and stress level on t_f. This function can be identified by studying the sensitivity of t_f to each one of the microscopic parameters and the stress level.

In this study SF means the highest Schmid factor among the basal and prism slip systems of the soft grain. To study the effect of SF and misorientation θ_{mis} on t_f, the model is adjusted such that the SF of the soft outer grain assumes the values 0.425, 0.45, 0.475, 0.49 and 0.5. The possible range of θ_{mis} values depends on the SF values. For lower values of SF, θ_{mis} can

Table 1
17 different combinations of SF and θ_{mis} considered for the crack nucleation parametric study.

SF	0.425	0.45	0.475	0.49	0.5
θ^o_{mis}	30.9	32	36.5	40	45
	46	45	40	45	
	60.5	55	52	50.8	
	67	60	60.5	56	

vary in a broader range, while for the highest possible Schmid factor of 0.5, θ_{mis} can just take the value of 45 degrees. Table 1 shows 17 different combinations of SF and θ_{mis} considered in this parametric study.

The grain size is defined as the diameter of an equivalent sphere with the same volume as the grain. The effect of grain size on load shedding response has been studied for various combinations of hard and soft grain sizes in (Venkataramani et al., 2007), where it was shown that the stress concentration due to load shedding is governed by the soft grain size. Varying the size of the hard grain does not have any appreciable effect on load shedding, as the $< c + a >$ slip systems, which get activated in the hard grain, have much higher slip system deformation resistance in comparison with the basal systems. An increase or decrease in slip system deformation resistance of $< c + a >$ system due to size effect relationship does not cause significant change to its already high values. The study of the effect of soft grain size is conducted on the RVE's with different combinations of SF, θ_{mis} and P for each grain size. For $SF = 0.5$ and $P = 650$ MPa different sizes from 7.5 to 100 mu m are considered for the soft grain. For other values of SF, three values of 7.5, 15, 30 μm are considered for the soft grain size.

The applied creep stress P is also expected to have a significant effect on crack nucleation in polycrystalline materials. For high stress creep tests the micro-crack nucleation due to load-shedding occurs earlier in comparison with low stress tests. To study the influence of P on t_f, the RVEs are subject to various stress levels in the range from 450 MPa to 950 MPa depending on other parameters. A total number of 183 CPFE creep simulations, followed by post-processing are performed for various combinations of SF, θ_{mis}, D and P. The natural log of the time to crack nucleation $Ln(t_f)$ is plotted as a function of creep stress P for different grain sizes D, viz. 7.5 μm, 15 μm and 30 μm, in Fig. 5. The time to crack nucleation varies inversely with P. Simultaneously, for any particular stress level, t_f reduces as the grain size increases. However, as the stress increases above 900 MPa, the influence of grain size on t_f reduces. Fig. 6 plots the variation of the time to crack nucleation (in log. scale) with grain size D, which is varied from 7.5 to 100 μm. The Schmid factor is maintained at 0.5, for which only one misorientation can be assumed, which is 45°. The time to crack nucleation drops with increasing grain size, as mentioned before. Fig. 7 plots the variation of the time to crack nucleation as a function of stress for different values of misorientation. It is observed that less macroscopic stress is required for crack nucleation at a particular time as the misorientation increases. Fig. 8 shows the effect of misorientation on the time to crack nucleation for different Schmid factors. The time decreases with increasing SF. At Schmid factor 0.5 the maximum resolved shear stress on the soft slip systems is attained and correspondingly, t_f is a minimum.

3.1. Functional Form of t_f in Terms of the Microstructural Parameters and the Stress Level

The values of the time to crack nucleation for the different RVEs and conditions are used to derive a functional form of t_f in terms of microstructural parameters (SF, θ_{mis} and D) and the macroscopic stress level (P). A power law functional form is assumed as:

$$Ln(t_f) = (A_1 + B_1\ SF^{\alpha})(A_2 + B_2\ \theta^{\beta}_{mis})(A_3 + B_3\ P^{\gamma})(A_4 + B_4\ D^{\eta}) \tag{19}$$

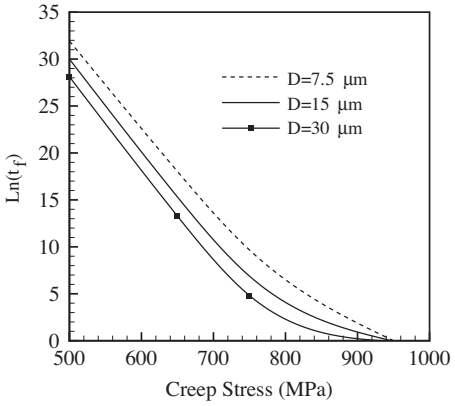

Fig. 5. Natural log of the time to crack nucleation (in secs.) as a function of the applied stress for different grain sizes ($SF = 0.45$ and $\theta_{mis} = 32^o$).

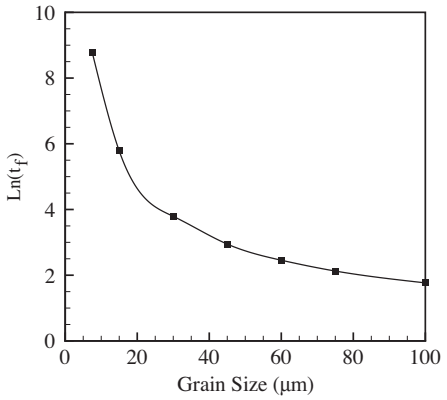

Fig. 6. Natural log of the time to crack nucleation (in secs.) as a function of grain size for $SF = 0.5, \theta_{mis} = 45^0$ and $P = 650$ MPa.

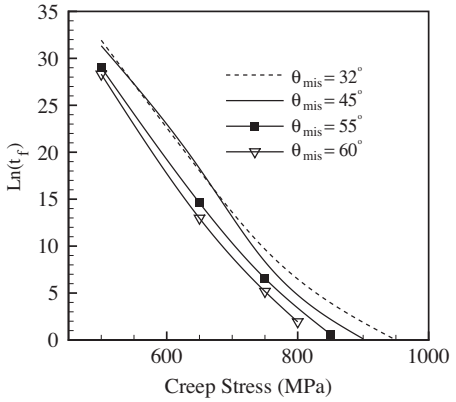

Fig. 7. Natural log of the time to crack nucleation (in secs.) as a function of stress for different misorientations corresponding to $SF = 0.45$ and $D = 7.5$ μm.

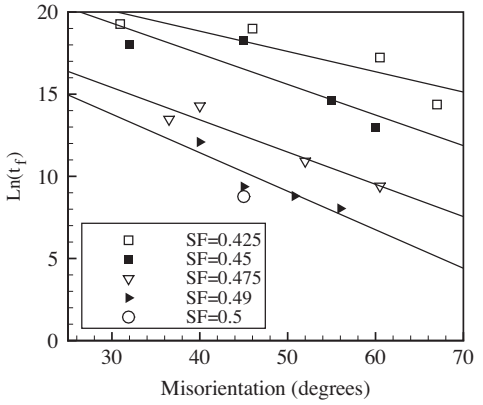

Fig. 8. Natural log of the time to crack nucleation (in secs.) as a function of misorientation for different Schmid factors ($P = 650$ MPa and $D = 7.5$ μm).

The parameters $A_i(i = 1, \ldots, 4), B_i(i = 1, \ldots, 4), \alpha, \beta, \gamma$ and η are obtained from a least square fit of the data from the 183 simulations with a correlation coefficient of $R^2 = 0.974$ as:

$$Ln(t_f) = (5.7 - 22.3SF^{2.6})(301.5 - 0.9\theta_{mis}^{1.2})\left(-0.008 + \frac{9.5}{P}\right)\left(2.7 + \frac{9.5}{D^{0.3}}\right) \tag{20}$$

In this model, the time t_f is in seconds, the misorientation is represented in degrees, the size D is in μm, and the stress P is in MPa. The coefficients $A_i(i = 1, \ldots, 4), B_i(i = 1, \ldots, 4)$ have appropriate units for dimensional consistency.

4. Probabilistic macroscopic crack nucleation model for polycrystalline ti alloys

The final goal is the development of a probabilistic macroscopic model of crack nucleation for implementation at the structural scale, from the function t_f established in Eq. (20) for Ti alloys. It is expected to predict the probability of crack nucleation at any point in the structure at any instant of loading, with known microstructural characteristics and macroscopic stress state at that point. The model accounts for the distribution of orientation (Schmid factor), misorientation and grain size, characterizing the microstructure at a point in the structure.

Fig. 9(a) shows a 0.2 m $\times$ 0.03 m cantilever beam that is loaded in plane strain by an applied moment of 0.11 kN m at the free end. The figure also shows the distribution of macroscopic stress σ_{xx} obtained from a FE simulation using the homogenized, anisotropic plasticity constitutive (HAPC) model developed in part 1 of this paper (Ghosh et al., in press). An underlying microstructural representative volume element or RVE at any point in this beam is shown in Fig. 9(b). The contour plot in this figure corresponds to the $< c >$-axis orientation of the grains. The macroscopic stress-state on this microstructural RVE can be obtained from the continuum-level HAPC-based FE results of Fig. 9(a). If the microstructure associated with the point was simply the two-grain system of Fig. 3(a), Eq. (20) can be readily used to deterministically calculate the time to crack nucleation at that point. However, the microstructure of Fig. 9(b) contains a large number of hard-soft grain combinations. Consequently, there are distributions of the microstructural parameters SF, θ_{mis} and D associated with the point, as opposed to a single value as in the two-grain RVE of Fig. 3(a). For each grain pair in the microstructure, a constituent grain is designated as hard or soft depending on the highest basal/prism Schmid factor. Subsequently, the microstructural descriptors SF, θ_{mis} and D are determined for each grain pair. A joint distribution function is subsequently generated for these parameters. The individual distribution functions for SF, θ_{mis} and D for a sample microstructure are plotted in Figs. 9(c), (d) and (e), respectively. The distribution functions are shown with respect to the contact area fraction of grain pairs, signifying that grain-pairs with larger contact area are weighted more heavily.

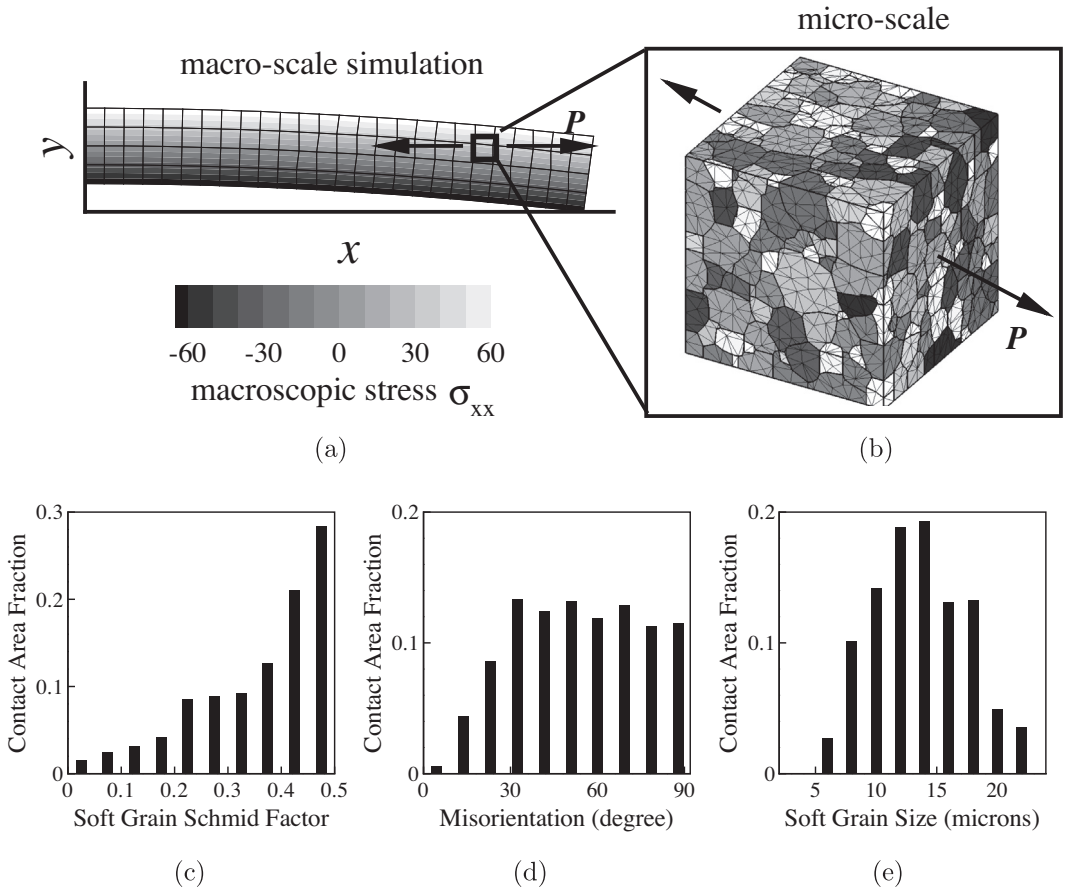

Fig. 9. (a) Distribution of macroscopic stress σ_{xx} in a cantilever beam obtained from a continuum-level FE simulation subject to transverse creep loading, (b) microstructural RVE corresponding at a material point in the cantilever beam, (c) distribution of soft grain Schmid factor, (d) distribution of misorientation, (e) distribution of soft size for a sample microstructure.

Suppose that there are N grain-pairs in the microstructure. Consider the i^{th} grain pair in the microstructure with descriptors SF^i, θ^i_{mis} and D^i. If the microstructure included only this grain pair, the time to failure would be equal to t^i_f, where

$$t^i_f = exp\left[\left[5.7 - 22.3(SF^i)^{2.6}\right]\left[301.5 - 0.9(\theta^i_{mis})^{1.2}\right]\left[-0.008 + \frac{9.5}{\sigma_{max}}\right]\left[2.7 + \frac{9.5}{(D^i)^{0.3}}\right]\right] \tag{21}$$

Here σ_{max} is the maximum principal macroscopic stress obtained from continuum-level HAPC-FE simulations. It should be noted that Eq. (21) is applicable only when one of the principal macroscopic stress components is considerably larger than the other components, because this equation has been obtained from CPFE simulations of 2-grain system RVEs under uniaxial loadings. Correspondingly SF^i is calculated with respect to the direction of maximum principal stress σ_{max}. The contact area between i^{th} grain-pair C^i is assumed to be a primary marker, determining the time to crack nucleation. Since the i^{th} grain pair is one of N grain pairs in the ensemble, the probability of crack nucleation at $t = t^i_f$ is assumed to be:

$$\Pr|_{t=t^i_f} = \frac{C^i}{\sum_{I=1}^{N} C^I} \tag{22}$$

where C^I is the contact area between the constituent grains in the I^{th} grain pair. Here it should be noted that the definition of crack nucleation in the macroscopic model is different from that at the grain-level. Eq. (20) cannot be used to predict grain-level crack nucleation in the microstructure of Fig. 9(b) because of two reasons:

- Eq. (20) has been obtained for one hard-soft grain pair, where there is no influence of other grain pairs. However, in the microstructure of Fig. 9(b), nucleation in every grain pair location is affected by the state of other grain pairs in the ensemble.
- The applied stress on each grain pair of the microstructure is different from the macroscopic stress σ_{max}.

From Eq. (22) the probability of macroscopic crack nucleation occurring before a particular time t^* is then expressed as:

$$\Pr|_{t\leqslant t^*} = \frac{\sum_{I=1} C^I}{\sum_{J=1}^{N} C^J} \quad \text{where } I \in \mathbf{g}^* \tag{23}$$

Here $\mathbf{g}^*$ is the set of all grain pairs I for which $t^I_f \leqslant t^*$, where t^I_f is evaluated from Eq. (21). It should be emphasized that the present model does not incorporate any changing topology due to propagation of the nucleated cracks, and there is no stress redistribution due to crack evolution in the microstructure. Hence, the macroscopic nucleation model ignores the effect of stress redistribution after crack initiation.

4.1. Validation of the macroscopic crack nucleation model

A post-processing code is developed using Eq. (23) to determine the probability of macroscopic crack nucleation for a given microstructure under a specified creep load, as a function of time. The probability density function (PDF) of $Ln(t_f)$ for two sample microstructures, viz. M1 and M2 are obtained using this code, and plotted in Fig. 10(a). Both microstructures consist of $7 \times 7 \times 7$ cubic grains, which are discretized into a FE mesh of 16464 tetrahedron elements. The two microstructures have different distributions of SF, θ_{mis} and D as shown in Fig. 11(a–c). The microstructures M1 and M2 are subject to a creep load of $P = 800$ MPa. Fig. 10(b) shows the cumulative density function (CDF) of $Ln(t_f)$ for these microstructures, derived using Eqs. (23) and (21). At any given time, the probability of macroscopic crack nucleation for M1 is lower than that for M2. The macroscopic crack nucleation model is validated for these simple microstructures by comparing with results of microstructural CPFE simulations using a procedure, discussed next.

- CPFE simulations are performed for the sample microstructures M1 and M2 under a uniaxial creep load of $P = 800$ MPa.
- The results of the CPFE simulations are post-processed to predict grain-level crack nucleation for the two microstructures using the microscopic model of Eq. (4) in Section 2. A hard grain boundary crack nucleates in a hard-soft grain pair when the effective nucleation parameter R at that grain pair reaches the critical value $R_c = 178.7\ \text{MPa}\sqrt{\mu\text{m}}$. The results of the CPFE simulations can be used, along with the failure criterion of Eq. (4), to predict the number of crack nucleation locations as a function of time. Fig. 12(a) shows the number of crack nucleation locations as a function of time (in the log. scale) for the two microstructures. At any given time, the number of crack nucleation locations is higher for microstructure M2 than for M1. This is consistent with the plots of CDF of $Ln(t_f)$ for M1 and M2 in Fig. 10(b), where the probability of macroscopic crack nucleation is higher for M2 at any instance of time.
- For a realistic interpretation of macroscopic crack nucleation, the probability of this macroscopic crack nucleation at a given time may be assumed to be a function of the number of grain-level crack nucleation sites. The results obtained for the microstructure M2 in Figs. 10(b) and 12(a) may be used to establish this relationship. For example, from Fig. 12(a), the third crack nucleation for M2 occurs at $Ln(t) = 7.2$. The corresponding probability of macroscopic crack nucleation for M2 at this time from Fig. 10(b) is 0.88. Thus, the occurrence of 3 grain-level microscopic cracks in CPFE simulations corresponds to a 88% probability of macroscopic nucleation. This relation is established in Fig. 12(b), which

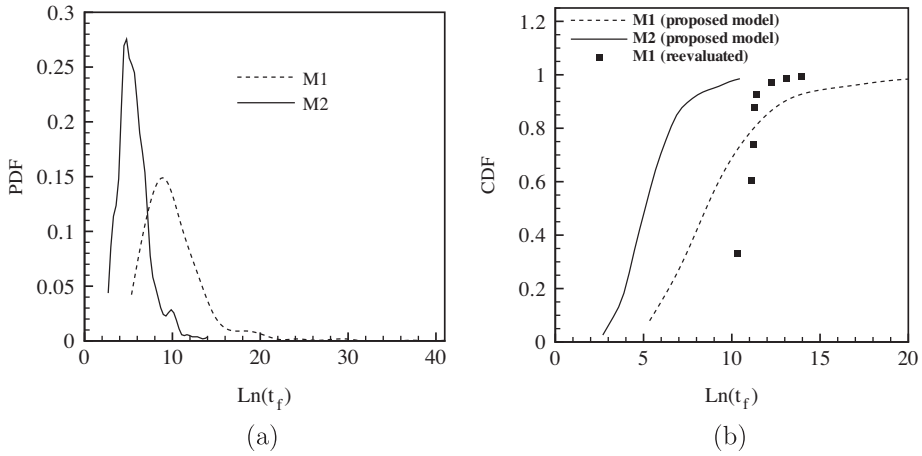

Fig. 10. Statistical distribution functions of $Ln(t_f)$ for sample microstructures M1 and M2: (a) probability density function (PDF), (b) cumulative density function (CDF).

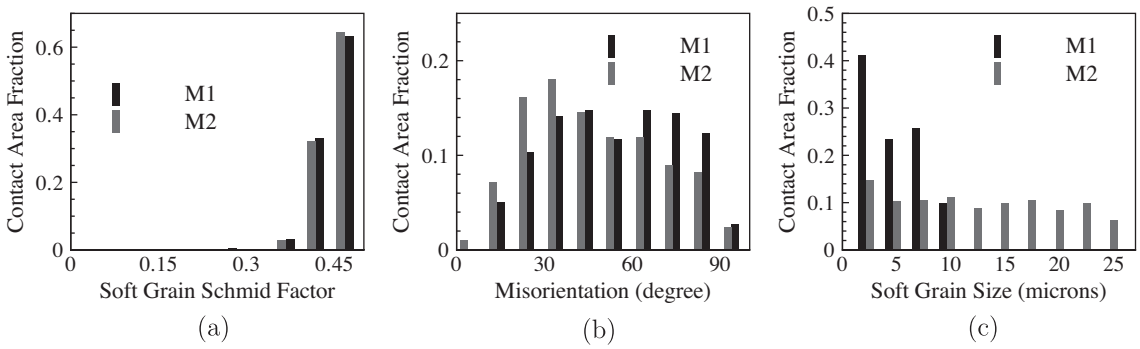

Fig. 11. Distributions of (a) soft grain Schmid factor, (b) misorientation and (c) soft grain size for sample microstructures M1 and M2.

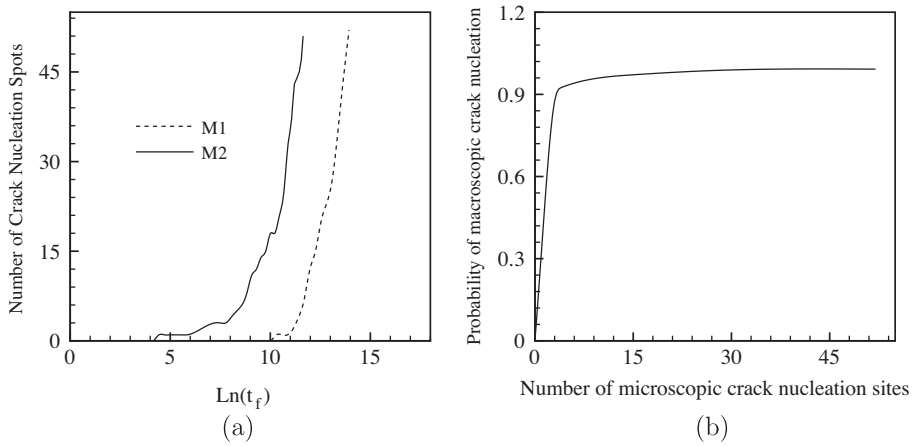

Fig. 12. (a) Number of crack nucleation sites as a function of time (in the log. scale) for microstructural samples M1 and M2, obtained by using the microscopic crack nucleation model of Section 2, (b) probability of macroscopic crack nucleation as a function of number of microscopic crack nucleation sites.

shows the probability of macroscopic crack nucleation as a function of the number of microscopic crack nucleation sites in the polycrystalline microstructure. The macroscopic crack probability distribution saturates at near unity values for 7–9 microscopic crack nucleation sites.

- To test the effectiveness of the functional relation in Fig. 12(b), the plots in Figs. 12(a) and (b) are used to re-evaluate the cumulative density function of $Ln(t_f)$ for the sample M1 and compare this with the original CDF obtained from Eq. (23). For example, based on Fig. 12(a), the third crack nucleation for M1 occurs at $Ln(t) = 11.28$. This occurrence of three microscopic cracks corresponds to a probability of macroscopic crack nucleation of 0.88 in Fig. 12(b). Thus, there is a 88% probability of macroscopic crack nucleation for M1 at $Ln(t) = 11.28$. Fig. 10(b) compares the re-evaluated CDF of $Ln(t_f)$ for M1 with the original one obtained from the proposed macroscopic crack nucleation model in Eq. (23). The two results generally show reasonable agreement.

The results in this study affirm the effectiveness of this microstructural physics-based approach to establish the probability of crack nucleation in a structure that is comprised of a polycrystalline metallic microstructure. While more detailed studies may be conducted with multi-axial loading cases leading to more complex functional relations, the present study achieves its desired goal of incorporating important microstructural features in models of fatigue crack nucleation. This field needs physics-based models of this class to overcome the limitations of pure macroscopic and statistical approaches.

5. Conclusion

The second part of this two part paper develops a macroscopic probability-based fatigue nucleation model from crystal plasticity FE-based microscopic fatigue crack nucleation results in polycrystalline microstructures of Ti alloys. The goal of this model is to predict macroscopic crack nucleation from structural-scale finite element simulations using the homogenized, anisotropic plasticity constitutive (HAPC) model developed in the first part (Ghosh et al., in press), given the microstructural characteristics and the local stress state. The probability of this macroscopic crack nucleation is quantified in terms of the number of microscopic crack nucleation sites.

Development of the macroscopic crack nucleation model proceeds in two stages. In the first stage, a physics-based grain level crack nucleation model in conjunction with crystal plasticity FE simulations of polycrystalline microstructures (Anahid et al., 2011; Ghosh et al., 2011) is used to arrive at a deterministic functional form relating the time to crack initiation t_f with the macroscopic stress state and microstructural characteristic parameters. CPFE models, representing a range of crystallographic and morphological characteristics for a two-grain ensemble, are used to calibrate this functional form. In the second stage, a probabilistic model for expected crack nucleation at any location in the structural scale is generated by using this functional form. The probability is expressed in terms of the local morphology, e.g. distribution functions of orientation, misorientation and grain size. A unique aspect of this model is that it makes a direct connection of the structural scale nucleation to the physics and mechanisms of microstructural crack nucleation process. This aspect is largely missing in the literature. The model developed in this paper can be extended to incorporate multi-axial loading cases by conducting other loading cases like bi/tri-axial tension and compression, shear etc. While such extensions will make the models more complicated, the framework is not expected to change significantly.

Acknowledgments

This work has been supported by the Air Force Office of Scientific through a Discovery Challenge Grant (DCT Grant # FA-9550-09-1-045 2, Program Manager: Dr. David Stargel). This sponsorship is gratefully acknowledged.

References

Anahid, M., Chakraborty, P., Joseph, D.S., Ghosh, S., 2009. Wavelet decomposed dual-time scale crystal plasticity FE model for analyzing cyclic deformation induced crack nucleation in polycrystals. Model. Simul. Mater. Sci. Eng. 37, 064009.

Anahid, M., Samal, M.K., Ghosh, S., 2011. Dwell fatigue crack nucleation model based on crystal plasticity finite element simulations of polycrystalline titanium alloys. J. Mech. Phys. Solids 59 (10), 2157–2176.

Bache, M.R., 2003. A review of dwell sensitive fatigue in titanium alloys: the role of microstructure, texture and operating conditions. Int. J. Fatigue 25, 1079–1087.

Bache, M.R., Cope, M., Davies, H.M., Evans, E.J., Harrison, G., 1997. Dwell sensitive fatigue in a near alpha titanium alloy at ambient temperature. Int. J. Fatigue 19 (93), 83–88.

Bennett, V.P., McDowell, D.L., 2003. Polycrystal orientation distribution effects on microslip in high cycle fatigue. Int. J. Fatigue 25, 27–39.

Bieler, T.R., Eisenlohr, P., Roters, F., Kumar, D., Mason, D.E., Crimp, M.A., 2009. The role of heterogeneous deformation on damage nucleation at grain boundaries in single phase metals. Int. J. Plasticity 25, 1655–1683.

Bridiera, F., McDowell, D.L., Villechaise, P., Mendeza, J., 2009. Crystal plasticity modeling of slip activity in Ti–6Al–4V under high cycle fatigue loading. Int. J. Plasticity 25, 1066–1082.

Coffin, L.F., 1973. Fatigue. Ann. Rev. Mat. Sci. 2, 313–348.

Engelen, R.A.B., Geers, M.G.D., Baaijens, F.P.T., 2003. Nonlocal implicit gradient-enhanced elasto-plasticity for the modeling of softening behavior. Int. J. Plasticity 19, 403–433.

Fleck, N.A., Kang, K.J., Ashby, M.F., 1994. The cyclic properties of engineering materials. Acta Met. Mater. 42, 365–381.

Ghosh, S., Anahid, M., in press. Homogenized constitutive and fatigue nucleation models from crystal plasticity fe simulations of ti alloys, part 1: Macroscopic anisotropic yield function. Int. J. Plasticity

Ghosh, S., Anahid, M., Chakraborty, P., 2011. Modeling fatigue crack nucleation using crystal plasticity finite element simulations and multi-time scaling. In: Ghosh, S., Dimiduk, D. (Eds.), Computational Methods for Microstructure-Property Relationships. Springer, New York, Dordrecht, Heidelberg, London, pp. 497–554.

Goh, C.H., Wallace, J.M., Neu, R.W., McDowell, D.L., 2001. Polycrystal plasticity simulations of fretting fatigue. Int. J. Fatigue 23, 5423–5435.

Kirane, K., Ghosh, S., 2008. A cold dwell fatigue crack nucleation criterion for polycrystalline Ti-6242 using grain-level crystal plasticity FE model. Int. J. Fatigue 30, 2127–2139.
Kirane, K., Ghosh, S., Groeber, M., Bhattacharjee, A., 2009. Crystal plasticity finite element based grain level crack nucleation criterion for Ti-6242 alloys under dwell loading. J. Eng. Mater. Tech. ASME 131, 27–37.
Laird, C.M., 1976. The fatigue limit of metals. Mater. Sci. Eng. 22, 231–236.
Liu, Y., Mahadevan, S., 2009. Probabilistic fatigue life prediction using an equivalent initial flaw size distribution. Int. J. Fatigue 31, 476–487.
McClung, R.C., Enright, M.P., Millwater, H.R., Leverant, G.R., Hudak, S.J., 2004. A software framework for probabilistic fatigue life assessment of gas turbine engine rotors. J. ASTM Int. 1 (8), 1371–1388.
McDowell, D., Dunne, F.P.E., 2010. Microstructure-sensitive computational modeling of fatigue crack formation. Int. J. Fatigue 32, 1521–1542.
Mineur, M., Villechaise, P., Mendez, J., 2000. Influence of the crystalline texture on the fatigue behavior of a 316L austenitic stainless steel. Mater. Sci. Eng. A286, 257–268.
Owolabi, G.M., Prasannavenkatesan, R., McDowell, D.L., 2010. Probabilistic framework for a microstructure-sensitive fatigue notch factor. Int. J. Fatigue 32, 1378–1388.
Paris, P.C., 1964. The fracture mechanics approach to fatigue, fatigue an interdisciplinary approach. Syracuse University Press, Syracuse.
Parvatareddy, H., Dillard, D.A., 1999. Effect of mode-mixity on the fracture toughness of Ti-6Al-4V/FM-5 adhesive joints. Int. J. Fracture 96, 215–228.
Pilchak, A.L., Williams, J.C., 2011. Observations of facet formation in near α titanium and comments on the role of hydrogen. Metall. Mat. Trans. A 42, 1000–1027.
Przybyla, C.P., McDowell, D.L., 2010. Microstructure-sensitive extreme value probabilities for high cycle fatigue of ni-base superalloy in100. Int. J. Plasticity 26, 372–394.
Przybyla, C.P., McDowell, D.L., 2011. Simulated microstructure-sensitive extreme value probabilities for high cycle fatigue of duplex ti-6al-4v. Int. J. Plasticity 27, 1871–1895.
Ruiz, G., Pandolfi, A., Oritz, M., 2001. Three-dimensional cohesive modeling of dynamic mixed mode fracture. Int. J. Numer. Methods Eng. 52, 97–120.
Sackett, E., Germain, L., Bache, M., 2007. Crystal plasticity, fatigue crack initiation and fatigue performance of advanced titanium alloys. Int. J. Fatigue 29, 2015–2021.
Sinha, S., Ghosh, S., 2006. Modeling cyclic ratcheting based fatigue life of HSLA steels using crystal plasticity fem simulations and experiments. Int. J. Fatigue 28, 1690–1704.
Sinha, V., Mills, M.J., Williams, J.C., 2004. Understanding the contributions of normal-fatigue and static loading to the dwell fatigue in a near-alpha titanium alloy. Metall. Mat. Trans. A 35, 3141–3148.
Sinha, V., Mills, M.J., Williams, J.C., 2006a. Crystallography of fracture facets in a near alpha titanium alloy. Metall. Trans. A. 37A, 2015–2026.
Sinha, V., Spowart, J.E., Mills, M.J., Williams, J.C., 2006b. Observations on the faceted initiation site in the dwell-fatigue tested Ti-6242 alloy: crystallographic orientation and size effects. Metall. Trans. A. 37A, 1507–1518.
Stroh, A.N., 1954. The formation of cracks as a result of plastic flow. Proc. R. Soc. London Ser. A 223, 404–414.
Suresh, S., 1998. Fatigue of Materials. Cambridge University Press, Cambridge.
Turkmen, H.S., Loge, R.E., Dawson, P.R., Miller, M., 2003. On the mechanical behavior of aa 7075-t6 during cyclic loading. Int. J. Fatigue 25, 267–281.
Venkataramani, G., Ghosh, S., Mills, M.J., 2007. A size dependent crystal plasticity finite element model for creep and load-shedding in polycrystalline Titanium alloys. Acta Mater. 55, 3971–3986.